Horizontal flow and surface patterns in a vertically vibrated annular granular layer

Hui Cai,[1,2] Weizhong Chen,[1] and Guoqing Miao[1,*]

[1]*Institute of Acoustics and Key Laboratory of Modern Acoustics of Ministry of Education, Nanjing University, Nanjing 210093, People's Republic of China*

[2]*School of Electrical Engineering, Yancheng Institute of Technology, Yancheng 224051, People's Republic of China*

A set of experiments was carried out on the motion of granular materials in a vertically vibrated annular system with a sawtooth-shaped base. We observed the coexistence of granular flow and surface patterns such as periodic subharmonic waves and kink pairs. Different patterns can transit each other as control parameters vary. The flow varies with space and time, and oppositely directed flows can occur at different levels and different moments. The magnitude and direction of the flow depend on the parameters defining the system in a complex manner. The motion of the patterns relates to the granular flow in a different way from that in which the wave in an ordinary fluid relates to the moving fluid. A preliminary explanation is given to our experimental findings.

I. INTRODUCTION

To date, an increasing number of unusual properties in granular materials have been recognized [1–3]. Of particular interest in this respect are the dynamics of vibrated granular materials [4–6], which exhibit stationary states as well as waves and complex patterns. For instance, the convection, the heaping, and the surface waves, etc., were found and explored earlier [7]. It was then found that horizontal migration and size segregation were produced in a vertically vibrated granular system with a sawtooth-shaped base [8–10]. Furthermore, if the granular system is confined to an annular region with a sawtooth-shaped base between two upright cylinders, a horizontal flow is observed, both in experiments and computer simulations [11–13], in which the flow magnitude and direction depend on many parameters defining the system. This is explained as a macroscopic realization of thermal ratchets [14–16]. In fact, when the granular materials are subjected to a vertical vibration on the sawtooth-shaped base, both the horizontal flow and the surface patterns appear often simultaneously [17]. In Ref. [18], using white-noise excitation or a signal with specific frequency range to eliminate any convective or collective motions of the granules, the horizontal flow was analyzed with respect to many asymmetries. In Ref. [13], the horizontal flow was calculated at a specific moment of the vibration. In this paper, we investigate the motion of granular materials in a vertically vibrated annular system with a sawtooth-shaped base, paying particular attention to the coexistence of horizontal flow and surface patterns.

II. EXPERIMENTAL SETUP

In the experiments, we use aluminum spheres with a diameter of 3.0 ± 0.05 mm as a granular medium. The annular container with an average diameter of 187.5 mm, a height of 95 mm, and a width of 3.3 mm makes the granular layer within it two-dimensional. The container is made of transparent Plexiglas and has a sawtooth-shaped base. Each tooth is triangular, with a left side measuring 10 mm, a

right side 6 mm, and a base 10 mm. The thickness of the granular layer is $H \approx 7.0$. (We define $H = N/n$, where N is the total number of particles and n is the number of particles in a single layer.) The container is mounted on a Brüel & Kjær 4805 vibration exciter. The vibrator performs the vertical vibration $z(t) = A \sin 2\pi f t$, where A and f are the driving amplitude and driving frequency, respectively. We define the dimensionless driving acceleration amplitude $\Gamma = 4\pi^2 f^2 A/g$, and use f and Γ as two control parameters. f is changed from 14 to 24 Hz in steps of 1 Hz, and Γ from 3.2 to 6.4 in steps of 0.1.

III. SURFACE PATTERNS

A. Method

In order to study the motion of surface patterns, a DV camera (Panasonic NV-GS400) is used to record panoramic views of the granular layer. By playing back the videos of these panoramic views slowly, it is able to observe the patterns, for instance, the ordinary periodic subharmonic waves, the kink-antikink pairs (abbreviated kink pairs in the following), and the superpositions of kink pairs and subharmonic waves formed in the granular layer. Figure 1 represents the phase diagram of surface patterns on the $f \sim \Gamma$ plane. Figure 2 shows some typical surface patterns. The formation and transition of patterns are similar to those in Ref. [17] and are briefly reviewed here.

B. Surface patterns

If we fix the frequency at a certain value and increase the driving acceleration, when $\Gamma > 3.2$, a periodic subharmonic wave with half the driving frequency appears in the granular layer [Fig. 2(a)]. The amplitude of the subharmonic wave increases with Γ. When Γ approaches 4.4, the subharmonic wave becomes unstable and is gradually extinguished. A kink pair is then gradually formed [Fig. 2(b)]. The two arms of the kink pair oscillate out of phase in a vertical direction, with half the driving frequency and amplitude gradually increasing. When Γ exceeds 4.4, the kink pair becomes more stable and vigorous, and moves anticlockwise from the top-down view. Its velocity decreases with Γ. As Γ increases further, the kink
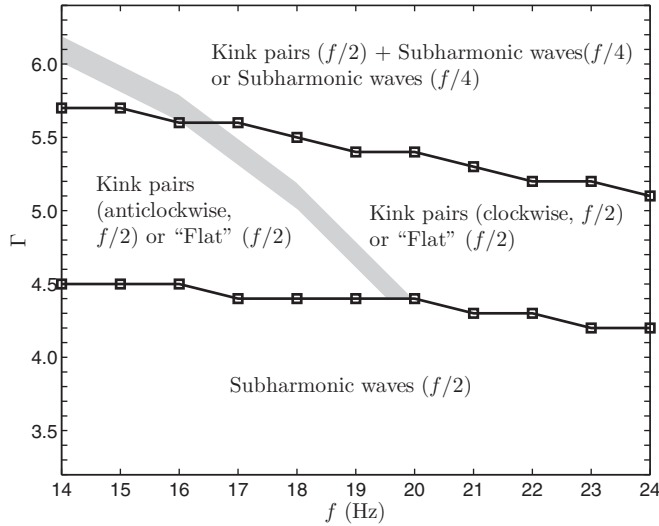
---

*miaogq@nju.edu.cn

FIG. 1. Phase diagram showing surface patterns. The shaded area represents a transitional region between anticlockwise kink pairs and clockwise kink pairs.

pair moves back and forth mostly, or rests occasionally [20]. If clockwise is defined as a positive direction, then the velocity of the kink pair increases with Γ. As Γ increases, the kink pair moves clockwise with the velocity increasing with Γ. Then for
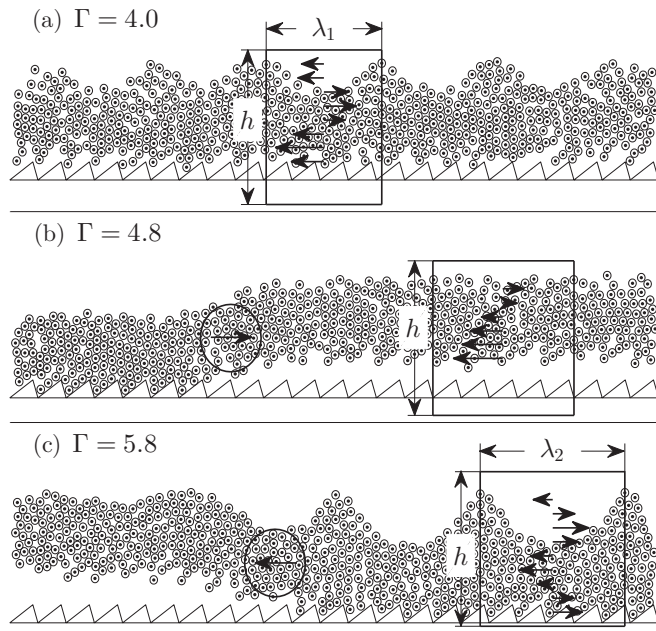

FIG. 2. Typical surface patterns recorded using a high-speed digital camera (Redlake MASD Motionscope PCI 2000 SC) and processed using an image technique [19] for $f = 18$ Hz: (a) periodic subharmonic wave, (b) anticlockwise kink pair, and (c) superposition of clockwise kink pair and subharmonic wave. The rectangle on each surface pattern represents the measure window in which the granular flow is measured. h is the height of the measure window. λ_1 and λ_2 are the wavelengths of subharmonic waves. The arrows in each measure window represent the schematic spatial flow distribution. The circles and the arrows in the circles represent the nodes and the directions in which they move, respectively.

the higher Γ, the kink pair becomes unstable. Instead, one kink pair, two kink pairs, and even three kink pairs form occasionally and transit mutually. The reason for the formation of kinks always in pairs is that the patterns in an annular container must satisfy the periodic condition. Above $\Gamma = 5.5$, a subharmonic wave with a quadruple driving period emerges in the two arms of the kink pair [Fig. 2(c)]. This state persists until $\Gamma = 6.4$. It is worth mentioning here that, in the regions where kink pairs appear, another kind of pattern, the "flat" surface pattern, may also appear instead of the kink pairs. The "flat" surface pattern is a form of motion in which the granular layer, as though it is a single body with a flat surface, vibrates vertically with half the driving frequency [21]. It either forms as soon as the driving parameters are fixed or evolves from unstable kink pairs by merging adjacent nodes until they all disappear. The appearance of a kink pair or a "flat" surface pattern is closely related to the process in which Γ is increased. If Γ is increased slowly, a kink pair is formed, while with a fast increment in Γ a "flat" surface pattern is more often formed. For the same reason, in the region of kink pair-subharmonic wave superpositions, if Γ is increased slowly, a superposition of kink pair and subharmonic wave is always formed, while with the fast increment in Γ a subharmonic wave with a frequency of $f/4$ is formed.

The formation and transition of the patterns described above evidently take place only in the range of 16 Hz $< f <$ 20 Hz. Beyond this range, the processes are more or less blurred. When $f \leqslant 16$ Hz, there are no clockwise kink pairs, but patterns in which an anticlockwise kink pair and subharmonic wave are superposed. We can see from Fig. 1 that, at lower frequencies, the anticlockwise kink pairs can exist over a larger range of Γ. For $f \geqslant 20$ Hz, there are no anticlockwise kink pairs.

C. Velocity of the kink pair

We, then, measured the velocity of the kink pairs v_k. Figure 3 shows that v_k is a monotonic increasing function of Γ for different f values. In cases where $f = 16$ and 18 Hz,
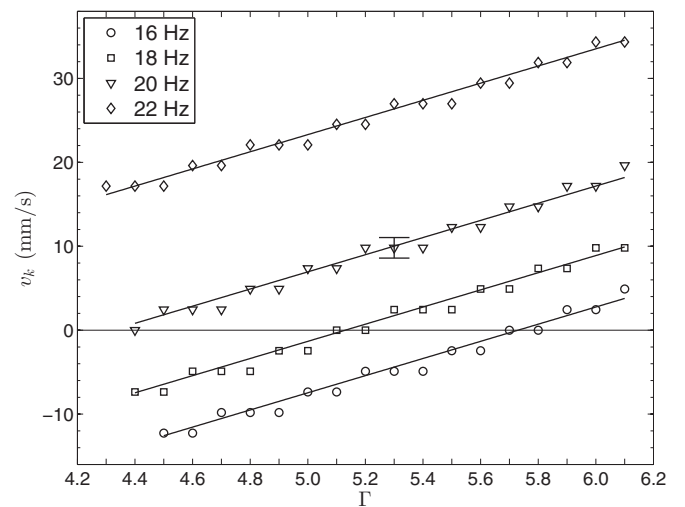

FIG. 3. v_k as a function of Γ for different f's. The markers represent the experimental results. Each curve represents a linear fit for the experimental results.
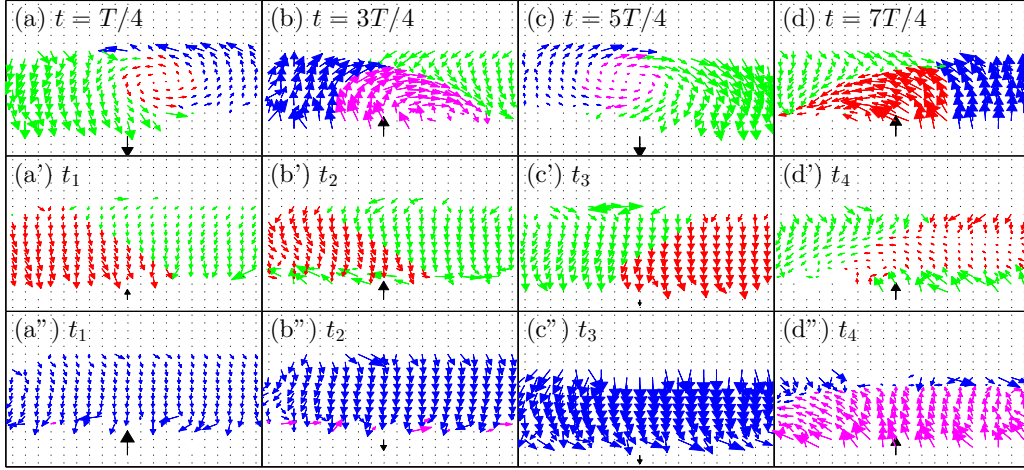
FIG. 4. (Color online) Velocity fields for $f = 20$ Hz. (a)–(d) A node region of a clockwise kink pair for $\Gamma = 5.4$. (a')–(d') One wavelength from a subharmonic wave for $\Gamma = 4.0$. (a")–(d") An arm region of a clockwise kink pair for $\Gamma = 5.0$. The lowest arrow in each subgraph represents the motion of the base in a vertical direction.

as Γ increases, the direction of the motion of the kink pair gradually changes from negative to positive. At about $\Gamma = 5.7$ (for $f = 16$ Hz) and 5.1 (for $f = 18$ Hz), the kink pair remains in a certain position. For cases where $f = 20$ and 22 Hz, the kink pair moves always in a positive direction. The maximum a v_k can reach is 3.5 perimeters of the channel per minute for $f = 22$ Hz and $\Gamma = 6.1$.

IV. HORIZONTAL FLOW

A. Method

In order to study the granular flow, we use a high-speed digital camera (Redlake MASD Motionscope PCI 2000 SC) to record the motion of the granules. A phase-lock frequency multiplication circuit is used to generate external trigger signals, controlling the high-speed digital camera recording at a rate of 20 frames per driving period. The spatial resolution of the high-speed camera is 320×280 pixels, with each pixel representing approximately 0.23 mm^2. A high-speed image-processing technique is then used to track the motion of the granules [19].

For each group of control parameters, 4000 frames are recorded every time and repeated at least three times. We could not record the motions of all the granules, as the field of view of the camera was limited. To overcome this difficulty, we noted the continuity of the stratified granular flow, that is, for the stratified granular flow, the total granular flow across any cross section along the circumference of the annular granular layer and at any time is equivalent. To verify the continuity of the stratified flow, we recorded the motion of the granules in several different positions along the circumference of the container and obtained the same results for the total granular flow. The result obtained at any local measure window (abbreviated m-window in the following) is therefore equivalent to that of the entire granular layer. By using this method, we are able to obtain the total granular flow varying with time, the flow distribution with height at any given moment, etc.

Regarding the "flat" pattern, the m-window might have an arbitrary length in a horizontal direction. For the periodic

wave, we might choose an m-window with a length of one wavelength in a horizontal direction [Fig. 2(a)] and obtain the space-period-averaged flow. For the kink pair, however, due to the complexity of the flow distribution in the node region (velocity fields show that there is convection in every node region [Figs. 4(a)–4(d)] and that the motion of the granules in the node region is not only affected by the sawteeth, but also by the convection), we might choose the m-window at the arm region. When Γ is lower, the two arms of the kink pair become compact and vibrate like two objects with opposite phases, with the choice of the m-window being the same as the "flat" pattern, i.e., the m-window with an arbitrary length in a horizontal direction [Fig. 2(b)]. When Γ is higher, the two arms once again become fluid and a subharmonic wave with $f/4$ appears in the arms, forming the kink pair-subharmonic wave superposition. The choice of the m-window is the same as the periodic wave, i.e., the m-window with a length of one wavelength in a horizontal direction [Fig. 2(c)]. In all cases, the m-windows in a vertical direction cover the entire granular layer. We divide the m-window into N_x columns and N_y rows (or N_y levels), i.e., $N_x \times N_y$ cells, each with a width of δx and a height of δy. We define the stratified flow at the jth level and the moment $k\delta t$, $F_s(j,k) = \frac{1}{N_x} \sum_{i=1}^{N_x} \rho(i,j,k)v_x(i,j,k)\delta y$, and the total flow at the moment $k\delta t$, $F_t(k) = \sum_{j=1}^{N_y} F_s(j,k)$, where $k = 0,1,2,3,\ldots$ represents $0, \delta t, 2\delta t, 3\delta t, \ldots$ moments, respectively, $i = 1,2,3,\ldots,N_x$ represents the ith column of the m-window, $j = 1,2,3,\ldots,N_y$ the jth row of the m-window, $\delta t = T/20$ a sample interval with T being the driving period, ρ the particle number density distribution, and v_x the horizontal velocity distribution.

We turn, at this point, to a study of the horizontal flow in the granular layer. In the following paragraphs we describe the dependence of the total flow on time, the height distribution of the flow at several given moments, as well as the dependence of the time-averaged total flow (defined as $\overline{F_t} = \frac{1}{2T} \sum_{k=1}^{40} F_t(k)\delta t$) on the driving parameters. These relations provide comprehensive information concerning the horizontal flow in the granular layer.
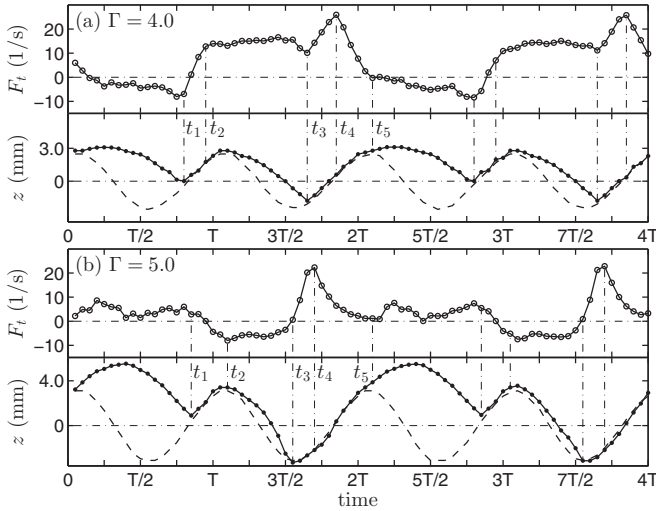
FIG. 5. Total flow in the granular layer and trajectory of the granular layer as a function of time for $f = 20$ Hz and two different Γ's: (a) $f/2$ subharmonic wave and (b) $f/2$ clockwise kink pair. In each subgraph, the upper figure represents the total flow versus time and the lower figure represents the trajectories of the layer (solid line, measured for vertical position of the lower boundary of the layer) and the base (dashed line) versus time. Here, $t = 0$ corresponds to the moment when the base reaches its highest point and $t = T/2$ the lowest point. Four driving periods are shown. The markers ($\circ$ and $\bullet$) on the lines indicate 20 sample points in every driving period.

B. F_t vs time

Figure 5 shows the total flow versus time. When Γ is lower, a subharmonic wave appears in the granular layer (cf., Fig. 1) first of all. We observed from the velocity fields [Figs. 4(a')–4(d')] that the two parts of the layer alternate in colliding with the base. At the moment t_1, the left part collides with the base [Fig. 4(a')]. The precollisional horizontal velocity of the lower level of this part is negative (here, the leftward direction is taken as positive), i.e., the lower level collides with the longer sides of the sawteeth on the base. After the layer-base collision, the lower level obtains a positive horizontal velocity. This results in a continuous increment in the granular flow from negative to positive during the layer-base collision. At the moment t_2, the layer separates from the base and flies freely [Fig. 4(b')]. The granular flow changes a little (see the relative flat region during the time interval $t_2 - t_3$). At the moment t_3, the right part collides with the base [Fig. 4(c')]. As in the first layer-base collision, the precollisional horizontal velocity of the lower level of this part is negative and the lower level obtains a positive horizontal velocity after the collision, resulting in a continuous increment in the positive granular flow. The period of this collision is longer than that of the first collision. Up to this point, it can be seen that, during the time interval $t_1 - t_3$, the granular layer with negative precollisional velocity collides with the longer sides of the sawteeth, obtaining a positive horizontal velocity after the collision. We call this the "positive ratchet effect." At the moment t_4, once it has separated from the longer sides of the sawteeth, the lower level collides with their shorter sides, obtaining a negative horizontal velocity [Fig. 4(d')].

This results in a continuous decrement of the granular flow until the moment t_5. We call this the "negative ratchet effect." The terms "positive ratchet effect" and "negative ratchet effect" are only used for convenience in the following analysis. Thus, during the whole period of the second layer-base collision, the granular flow undergoes a process during which its magnitude increases first and reaches a maximum at the moment t_4, decreasing thereafter. After separating from the base, the granular flow decreases very slowly due to the inelastic collisions occurring between granules until the next layer-base collision at the moment $t_1 + 2T$. When Γ is higher, a kink pair forms in the layer (cf., Fig. 1). Here, the granular flow is measured on one of the two arms [Fig. 2(b)]. At the moment t_1, the lower level of the layer has a positive precollisional horizontal velocity and collides with the shorter sides of the sawteeth [Fig. 4(a'')]. The total flow decreases fast during the whole first layer-base collision. After separating from the base at the moment t_2 [Fig. 4(b'')], the total flow remains negative with little change until the second layer-base collision occurs at the moment t_3 [Fig. 4(c'')]. During the second layer-base collision, the total flow increases first ($t_3 - t_4$) and then decreases ($t_4 - t_5$) as above [Fig. 4(d'')]. After separating from the base at moment t_5, the total flow also changes slowly until the next layer-base collision at moment $t_1 + 2T$. In Fig. 5, we can see periodic reversals of the total flow with time and different time-variation profiles of the total flow for different surface patterns. Layer-base collisions always lead to dramatic changes in the total flow.

C. F_s vs height

From the above, we can see that the fast variation of the granular flow always occurs when the layer collides with the base. Regarding the process of the layer-base collision, the lower level of the layer collides with the base first, then the variation of motion of the lower level is transferred upwards through collisions between granules. Or one can say, the periodic variation in the granular flow in the lower level is transferred upwards through an equivalent "shear force" between levels and shows some "wave" images. Figure 6 shows the height distribution of the stratified horizontal flow for an $f/2$ subharmonic wave and an $f/2$ kink pair at several given moments. Ordinarily, a positive and negative horizontal flow occur simultaneously in different levels of the layer. Like the total flow, the layer-base collision also causes changes in the spatial distribution of the horizontal flow. Corresponding to both the $f/2$ subharmonic wave and the $f/2$ kink pair, the variation period of the spatial distribution of the horizontal flow is also $2T$.

D. $\overline{F_t}$ vs Γ

In the following, we will study the variation of the time-averaged total flow with driving parameters. Figure 7 shows the time-averaged total flow versus the driving acceleration for different frequencies. The flow for each frequency always increases first, then decreases, and then, finally, increases once again. The first increment corresponds to the presence of a subharmonic wave in the granular layer, while the second increment corresponds to a clockwise kink pair with
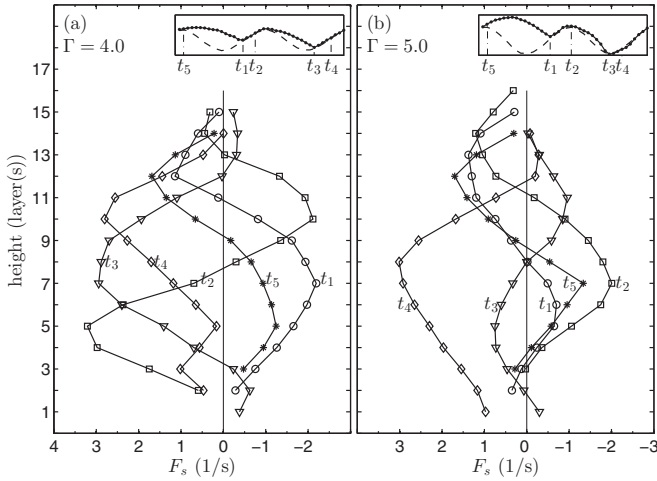
FIG. 6. Stratified horizontal flow in the granular layer as a function of height for several specific moments in one vibrating period for $f = 20$ Hz: (a) $f/2$ subharmonic wave and (b) $f/2$ clockwise kink pair. The inset of each subgraph shows the motions of the layer and the base in a vertical direction. The moments t_1, t_2, t_3, t_4, and t_5 correspond to those in Fig. 5, respectively.

an $f/4$ subharmonic wave in its arm. The variation of the time-averaged total flow with driving parameters could be explained as follows: the magnitude and direction of the time-averaged total flow are governed by two factors, the first being the ratchet effect and the second the fluidization of the layer. The reversals of the flow are governed by the ratchet effect, with the positive ratchet effect making the flow change from a negative to a positive direction, while the negative ratchet effect makes the flow change from a positive to a negative direction. The magnitude of the flow is governed by both ratchet and fluidization together. For a given f, increasing Γ from the value of 3.4 makes the layer vibrate with greater amplitude. The layer thus obtains more energy from the vibrating base, with the fluidization strengthening gradually. As a result, the flow in the layer increases with Γ. As Γ increases to a certain value, the layer becomes unstable and a kink pair is gradually formed in the layer. In this process, the fluidization in the arm region of the kink pair gradually becomes weaker than that for the subharmonic wave, with the flow gradually decreasing. With a further increment in Γ, the kink pair becomes more vigorous. When Γ reaches a certain value, a subharmonic wave with $f/4$ appears in the arm region and the fluidization strengthens gradually, with the flow again increasing. During the first increasing stage of the flow (Fig. 7), for a given Γ, increasing f makes the vibrating amplitude lower so that the fluidization becomes weaker and the flow correspondingly smaller; during the second increasing stage of the flow (Fig. 7), the layer becomes fully fluidized with the increasing f, resulting in a very palpable increment in the flow.

V. PATTERN-FLOW RELATION

We now turn to an analysis of the relation between the motions of the kink pair and the granular flow. Figure 8 shows the velocity of kink pair v_k versus the velocity of granular flow v_f. The values of Γ as parameters are marked next to some of the points. The data are from Fig. 7 (for v_f) and
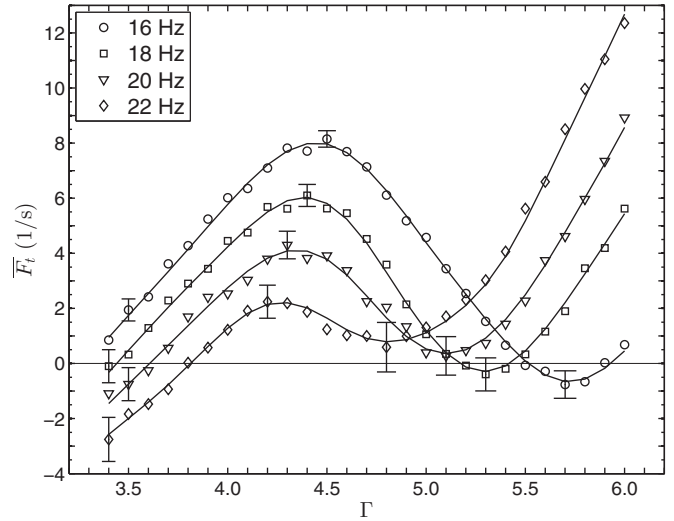

FIG. 7. Time-averaged total flow in the granular layer as a function of Γ for different f's. The markers represent the results of the experiments. Typical error bars are shown. Each curve represents a smoothing spline fit for the experimental results.

Fig. 3 (for v_k), respectively. Here, $v_f = \overline{F_t}/\overline{\rho}$, where $\overline{\rho} = \frac{1}{N_x N_y 2T} \sum_{k=1}^{40} \sum_{i=1}^{N_x} \sum_{j=1}^{N_y} \rho(i,j,k) \delta x \delta y \delta t$. The continuity and periodicity of the flow imply that v_f is independent of where it is measured. In Fig. 8, the minimum v_f for each frequency corresponds to the minimum $\overline{F_t}$ for the same f and Γ in Fig. 7. As far as $f = 20$ and 22 Hz are concerned, both the kink pair and granular flow move in a positive direction. As Γ increases from the values of 4.4 (for $f = 20$ Hz) and 4.3 (for $f = 22$ Hz), first of all, v_k increases as v_f decreases, and then both v_k and v_f increase with Γ after passing the minimum v_f. In the case of $f = 18$ Hz, as Γ increases from the value of 4.4, the kink pair moves in a negative direction while the granular flow moves in a positive direction. The
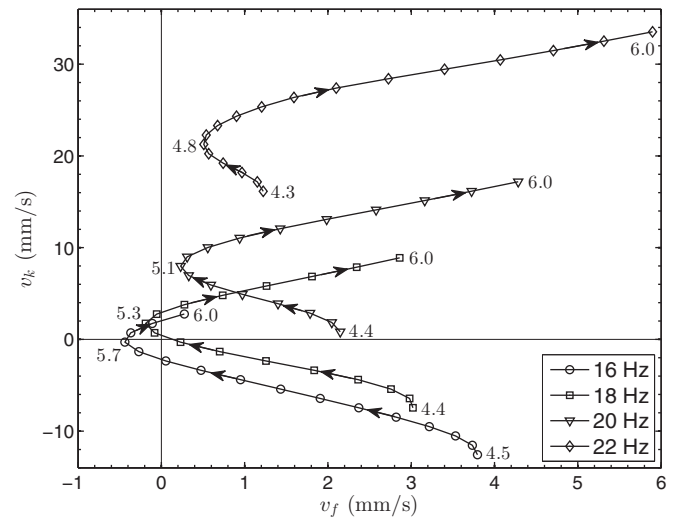

FIG. 8. Relation between v_k and v_f as Γ increases for different f's. The arrows on each curve indicate the direction in which Γ increases. The values of Γ as parameters are marked next to some of the points.

magnitude of their velocities both decrease gradually. When passing across $\Gamma = 5.1$, the direction taken by the motion of the kink pair is reversed and then moves in a positive direction. At about $\Gamma = 5.2$ and 5.4, the granular flow undergoes two reversals, with v_k increasing monotonically as Γ increases. Regarding $f = 16$ Hz, as Γ increases from a value of 4.5, the curve passes through the fourth, third, second, and first quadrants, consecutively. The kink pair and the granular flow undergo one reversal and two reversals of their velocities, respectively. From the above, we can see that the relation between the motions of the kink pair and the granular flow is both interesting and complex. It is different from the motion of the wave in an ordinary fluid related to a moving fluid.

VI. CONCLUSIONS

In summary, in this paper we have studied the coexistence of horizontal flow and surface patterns in a periodic granular system with a sawtooth-shaped vertically vibrated base. The phase diagram gives us a concrete and unambiguous picture of the formation and transition of the surface patterns. We have seen that under the vertical vibration of the sawtooth-shaped base, the granular layer fluidized. The granular flow (due to the ratchet effect caused by sawteeth on the base) and the surface patterns (due to the vertical vibration of the base) were formed simultaneously in the granular layer. The temporal-spacial distribution of the flow showed a periodicity which relates to the periodic vibration of the base. The granular flow and kink pair relate to driving parameters in different ways. This resulted in a complex relation between the motions of kink pair and granular flow. These interesting phenomena act as an encouragement to us to carry out a more thorough study in order to understand the precise nature of the motion of the granular materials under vertical vibration.

[1] Igor S. Aranson and Lev S. Tsimring, Rev. Mod. Phys. **78**, 641 (2006).

[2] G. D'Anna, P. Mayor, A. Barrat, V. Loreto, and Franco Nori, Nature (London) **424**, 909 (2003).

[3] Shahin Mobarakabadi, Ehsan Nedaaee Oskoee, Matthias Schröter, and Mehdi Habibi, Phys. Rev. E **88**, 042201 (2013).

[4] A. Götzendorfer, C. A. Kruelle, I. Rehberg, and D. Svenšek, Phys. Rev. Lett. **97**, 198001 (2006).

[5] J. E. Macías, M. G. Clerc, C. Falcón, and M. A. García-Ñustes, Phys. Rev. E **88**, 020201 (2013).

[6] P. Eshuis, D. van der Meer, M. Alam, H. J. van Gerner, K. van der Weele, and D. Lohse, Phys. Rev. Lett. **104**, 038001 (2010).

[7] H. M. Jaeger and S. R. Nagel, Science **255**, 1523 (1992); R. P. Behringer, Nonlinear Sci. Today **3**, 1 (1993).

[8] Xiaodong Shi, Guoqing Miao, and Hua Zhang, Phys. Rev. E **80**, 061306 (2009).

[9] Z. Farkas, F. Szalai, D. E. Wolf, and T. Vicsek, Phys. Rev. E **65**, 022301 (2002).

[10] S. J. Moon, D. I. Goldman, J. B. Swift, and H. L. Swinney, Phys. Rev. Lett. **91**, 134301 (2003).

[11] I. Derényi, P. Tegzes, and T. Vicsek, Chaos **8**, 657 (1998).

[12] Z. Farkas, P. Tegzes, A. Vukics, and T. Vicsek, Phys. Rev. E **60**, 7022 (1999).

[13] M. Levanon and D. C. Rapaport, Phys. Rev. E **64**, 011304 (2001).

[14] A. Gnoli, A. Petri, F. Dalton, G. Pontuale, G. Gradenigo, A. Sarracino, and A. Puglisi, Phys. Rev. Lett. **110**, 120601 (2013).

[15] V. Berardi, J. Lydon, P. G. Kevrekidis, C. Daraio, and R. Carretero-González, Phys. Rev. E **88**, 052202 (2013).

[16] P. Eshuis, K. van der Weele, D. Lohse, and D. van der Meer, Phys. Rev. Lett. **104**, 248001 (2010).

[17] Hui Cai, Weizhong Chen, and Guoqing Miao, Chin. Phys. Lett. **30**, 044501 (2013).

[18] R. Balzan, F. Dalton, V. Loreto, A. Petri, and G. Pontuale, Phys. Rev. E **83**, 031310 (2011).

[19] S. Warr, G. T. H. Jacques, and J. M. Huntley, Powder Technol. **81**, 41 (1994); R. D. Wildman and J. M. Huntley, *ibid.* **113**, 14 (2000).

[20] Peng Zhang, Guoqing Miao, Kai Huang, Yi Yun, and Rongjue Wei, Chin. Phys. Lett. **22**, 1961 (2005).

[21] F. Melo, P. B. Umbanhowar, and H. L. Swinney, Phys. Rev. Lett. **75**, 3838 (1995).